HHS Public Access

Author manuscript

Prog Biophys Mol Biol. Author manuscript; available in PMC 2021 March 03.

Published in final edited form as:

Prog Biophys Mol Biol. 2020 August ; 154: 62–70. doi:10.1016/j.pbiomolbio.2019.02.004.

Multimodal on-axis platform for all-optical electrophysiology with near-infrared probes in human stem-cell-derived cardiomyocytes

Aleksandra Klimas[1], **Gloria Ortiz**[2], **Steven Boggess**[2], **Evan W. Miller**[2,3,4], **Emilia Entcheva**[1,*]

[1]Department of Biomedical Engineering, The George Washington University, Washington, DC, 20052, USA

[2]Department of Chemistry, University of California, Berkeley, CA 94720, USA

[3]Department of Molecular & Cell Biology, University of California, Berkeley, CA 94720, USA

[4]Department of Helen Wills Neuroscience Institute, University of California, Berkeley, CA 94720, USA

Abstract

Combined optogenetic stimulation and optical imaging permit scalable, contact-free high-throughput probing of cellular electrophysiology and optimization of stem-cell derived excitable cells, such as neurons and muscle cells. We report a new “on-axis” configuration (combined single optical path for stimulation and for multi-parameter imaging) of OptoDyCE, our all-optical platform for studying human induced pluripotent stem-cell-derived cardiomyocytes (hiPSC-CMs) and other cell types, optically driven by Channelrhodopsin2 (ChR2). This solid-state system integrates optogenetic stimulation with temporally-multiplexed simultaneous recording of membrane voltage (V_m) and intracellular calcium ($[Ca^{2+}]_i$) dynamics using a single photo-detector. We demonstrate the capacity for combining multiple spectrally-compatible actuators and sensors, including newer high-performance near-infrared (NIR) voltage probes BeRST1 and Di-4-ANBDQBS, to record complex spatiotemporal responses of hiPSC-CMs to drugs in a high-throughput manner.

INTRODUCTION

Heart tissue is inherently dynamic, where a framework for both signal quantification and active interrogation is necessary to dissect the complex spatiotemporal phenomena underlying cardiac function [1]. Contraction of the heart is driven by the propagation of electrical waves. At the cellular level, the triggering event, an action potential (AP), is determined by the balance of inward (depolarizing) and outward (repolarizing) ionic

[*]*Contact for correspondence:* Emilia Entcheva, PhD, Department of Biomedical Engineering, George Washington University, 800 22nd St NW, Suite 5000, Washington, DC 20052, entcheva@gwu.edu.

currents; the AP is closely followed by the increase in intracellular calcium concentration in the form of calcium transients (CTs), and ultimately calcium mediates mechanical contraction. To better understand electrical dysfunction, which can lead to complex electrical disturbances known as arrhythmias, optical mapping provides a means of contactless, high spatiotemporal recording of activity in cardiac tissue by employing fluorescent reporters. AP signals are obtained using fluorescent membrane voltage (V_m) probes, such as the styryl dyes RH-237, Di-4-ANEPPS, and Di-8-ANEPPS, and intracellular calcium changes are captured by $[Ca^{2+}]_i$ -sensitive probes, such as Fura-2, Fluo-4 and Rhod-4, which typically provide stronger signals compared to the commonly used styrylbased V_m probes [2, 3]. When combined with spectrally-compatible optogenetic actuators, such as the genetically encoded depolarizing ion channel Channelrhodopsin2 (ChR2) [4] (Fig. 1a, b), dynamic events in cardiac electrophysiology can be interrogated in a fully contactless, highthroughput dynamic manner [5–7]. Dynamic space-time patterns of light can be imposed for control of excitation waves in cardiac tissue [8]. Optogenetic actuators can be combined with genetically-encoded sensors, such as the genetically-encoded calcium indicators (GECI) R- GECO [9] (Fig. 1b) and the GCaMP-family of calcium sensors [10] (when a spectrally-compatible version of ChR2 is used). Furthermore, they can be combined also with voltage-sensitive fluorescent proteins (VSFP) such as VSFP3 [11], the QuasAr2 [12], FlicR1 [13] and the ASAPs [14–17]. Newer red-shifted near-infrared (NIR) voltage-sensitive dyes, producing superior optical signals, such as Di-4-ANBDQBS [18] and BeRST1 [19], not only expand the palette of available sensors combinable with optogenetic actuators, but also enable simultaneous recording of V_m and $[Ca^{2+}]_i$ of optically interrogated samples when using greenexcited $[Ca^{2+}]_i$ probes.

The traditional tools for probing cardiomyocyte electrophysiology with embedded parallelism, such as the planar patch clamp systems [20] and microelectrode arrays (MEAs) [21], rely on contact-based interrogation. Patch-clamp systems are often limited to isolated/single cells [22] and/or (non-cardiac) cell lines. MEAs can work with cardiomyocyte syncytia and can record tissue-level properties, such as conduction velocity, yet the need for contact and the extracellular voltage readout present limitations. In contrast, the contactless nature of all-optical platforms, makes them suitable for probing of electrical activity in two- and three-dimensional constructs of human induced-pluripotent stem cells (hiPSC-CMs), i.e. allows them to investigate electrical activity within the tissue context. Our previously described system OptoDyCE exemplifies how optical mapping combined with optogenetics could be used to construct a low-cost, all-optical system for high-throughput cardiac electrophysiology. Here, we show the next generation of the OptoDyCE platform (Fig. 1c), where “on axis” design is used for optical stimulation and simultaneous V_m and $[Ca^{2+}]_i$ imaging in hiPSC-CMs onto a single detector with “strobed” LED illumination, gated to specific camera frames (Fig. 1d). The “on axis” configuration refers to the combined single optical path leading up to the sample for stimulation and for the multiparameter imaging. The resultant system is compact and fully compatible with standard multi-well plates (Fig. 1e).

In order to characterize and demonstrate the flexibility of the system, we compare multiple V_m and $[Ca^{2+}]_i$ probes in hiPSC-CMs. In addition to the more commonly used NIR V_m sensor Di-4-ANBDQBS, we show the first full characterization of a new NIR probe,

BeRST1, in optogenetically-paced hiPSC-CMs and demonstrate the compatibility of both sensors with ChR2 actuation as well as the $[Ca^{2+}]_i$ probes Rhod-4 and the genetically-encoded R-GECO. We assess the performance of the OptoDyCE platform and the utility of these probes for all-optical cardiac electrophysiology by quantifying spectral cross-talk due to the simultaneous use of multiple fluorescent probes and the stability of these probes under long-term, strobed illumination. To demonstrate the value of simultaneous dual imaging with high spatiotemporal resolution in the context of cardiotoxicity testing, we explore cell-level uncoupling between V_m and $[Ca^{2+}]_i$ in a known proarrhythmic compound, azimilide, in both spontaneous and opticallypaced conditions. By fully characterizing the presented all-optical platform, we show that when combined with hiPSC-CMs or other scalable experimental cardiac models, OptoDyCE can provide a high-throughput means of standardization of protocols for electrophysiology testing across multiple sites [23], cell sources [24] as well as multiple testing platforms [24, 25] with a high number of replicates making high-throughput drug discovery, disease modeling, and personalized medicine realizable.

MATERIALS AND METHODS

Human iPS-cardiomyocyte culture and gene delivery

Culture of hiPSC-CMs and adenoviral delivery of ChR2(H134R) was performed as described previously [5, 26, 27]. Briefly, frozen human iPSC-derived cardiomyocytes (iCell Cardiomyocytes^2 ™, Cellular Dynamics International (CDI), Madison, WI) were thawed per the manufacturer's instructions and plated on fibronectin-coated wells in 384-well glass-bottom plates (Cellvis, Mountain View, CA), Fig. 1e, at the recommended plating density of 156,000 cells/cm^2 (17,000 cells/well for a 384 well plate). After 5 days, adenoviral delivery of ChR2(H134R)-eYFP to the iPSC-CMs was performed in-dish at a viral dose of MOI 350. Transfection of R-GECO (Addgene #45494 (CMV-R-GECO1.2) developed by Robert Campbell) was performed in-dish after delivery of ChR2. Briefly, Lipofectamine 3000 (ThermoFisher, Waltham, MA), P3000 (ThermoFisher), CDI iCell Plating Medium, and the R-GECO plasmid were combined per manufacturer's instructions and plasmid-containing solution remained in each well for at least 48 hours. For all samples, functional testing was performed 2 days after transfection and/or infection.

All-optical recording of voltage and calcium under optogenetic pacing

Membrane voltage (V_m) and intracellular calcium ($[Ca^{2+}]_i$) sensitive probes were administered, as described previously [5, 28, 29]. All experiments were performed at room temperature in Tyrode's solution containing the following (in mM): NaCl, 135; MgCl2, 1; KCl, 5.4; CaCl2, 1.33; NaH2PO4, 0.33; glucose, 5; and HEPES, 5 at pH 7.4. Optical recording of V_m was performed using the new near-infrared synthetic dye BeRST1 [19] and Di-4-ANBDQBS (L. M. Loew) [18], while $[Ca^{2+}]_i$ was reported optically with Rhod-4 or R-GECO. All probes were spectrally-compatible with ChR2. Dyes were diluted in Tyrode's solution to the desired optimized concentration as follows: BeRST1 (1 μM), Di-4-ANBDQBS (35 μM), and Rhod-4 (10 μM). Optical imaging was performed at >200 frames per second (fps) with 4×4 binning with a field of view of ~0.4 mm^2 using NIS-Elements AR (Nikon Instruments; Melville, NY) on the OptoDyCE platform [6]. Recordings of

spontaneous and paced activity were obtained, where 5 ms, 0.5Hz optical stimulation (470 nm) was provided using supra-threshold irradiances, as needed (in all cases < 1mW/mm^2).

A schematic of the system control and data acquisition protocol along with the light path of the optical system can be seen in Fig. 1, similar to that described previously [5]. The optical system (Fig. 1c) was built around an inverted microscope (Nikon Eclipse TE-2000) fitted with a programmable x-y stage and automated z-focus (Prior Scientific; Rockland, MA), with illumination for actuation and sensing using a custom-built adaptor. Illumination for sensing was provided by red (sLED1, 640 mW, at 660 nm) for voltage and green (sLED2, 350 mW, at 530 nm) for calcium, respectively, controlled by LED drivers (all parts from Thorlabs). Both LEDs were fitted with a bandpass filter: F_{ex1}(Vm): FF655/40 nm (Semrock; Rochester, NY); F_{ex2} ($[Ca^{2+}]_i$): ET535/50 nm (Chroma; Bellows Falls, VT) and combined using a dichroic mirror DM1 (660 nm long-pass, Semrock). The actuation LED (aLED, 650 mW, 470 nm) for ChR2 was controlled using LED driver (Thorlabs) and fitted with a ET470/28 nm bandpass filter (Chroma), Factu. The light paths for optical sensing and actuation were combined by DM2 (495LPXR, Chroma) and directed to the sample using the appropriate dichroic DM3 for individual or simultaneous measurements (565DCXR, Chroma; 685-Di02, Semrock; 473/532/660rpc, Chroma). Irradiances between 0.3 – 6 mW/mm^2 for V and 0.05 – 1 mW/mm^2 for $[Ca^{2+}]_i$ were selected based on maximum signal strength while minimizing oversaturation of pixels and minimizing effects on ChR2 activation. Irradiances were chosen based on cell plating density and filter choice, but were kept constant over the course of a single experiment. In order to achieve simultaneous imaging, temporal multiplexing was used [30, 31], where sLED1 and sLED2 were gated to each camera frame. Collimation optics comprised of several lenses (L), and an objective lens (in this case 20x Nikon CFI Super Plan Fluor, NA 0.75) was used to direct light to the sample. Emitted fluorescence was collected by a photodetector (iXon Ultra 897 EMCCD; Andor Technology Ltd., Belfast, UK) after passing through the appropriate emission filter for individual or simultaneous measurements, F_{em} (ET605/70m; 700LP; ET595/40m +700LP, all Chroma). Illumination control was completely automated via software and TTL pulses. Illumination LEDs (sLED1 and sLED2) triggered off of the EMCCD camera (one LED on per frame during strobed illumination) and aLED was asynchronously controlled by an external TTL source (Fig. 1d).

Drug preparation

Azimilide is a class III anti-arrhythmic drug used often in patients with implantable devices to slow down rhythm. Azimilide was diluted in DMSO (Sigma Aldrich) to achieve concentrations of 0.01 – 10 mM when diluted in Tyrode's solution. After the sample plates were loaded with dye(s), the Tyrode's wash solution was removed and replaced with Tyrode's solution containing the compound. The plates were then returned to the incubator (37°C, 5% CO_2) for 30 minutes prior to experiments to allow for equilibration.

Data processing and analysis

Data was analyzed using software custom-developed in MATLAB [2, 5, 32], and the following endpoints were extracted: peak, percent change in fluorescence (ΔF/F%), and mean and standard deviation of baseline of V and [Ca^{2+}i] Signal-to-noise ratio (SNR) was

calculated as ratio of peak signal to the standard deviation of the signal baseline. All data was averaged over the whole camera field of view (400 mm × 400 mm), unless otherwise specified. Preprocessing included baseline correction, removal of artifacts, temporal filtering using a SavitzkyGolay polynomial filter (second order, 3 frame window) and normalization [32].

RESULTS

On-axis dual imaging system

The OptoDyCE system has been adapted to perform, for the first time, simultaneous dual imaging of voltage and calcium along with optogenetic stimulation using a single-detector, on-axis configuration (Fig. 1c). The choice of sensors and actuators is primarily limited by the spectral properties of the relevant chromophores (Fig. 1a). Currently, dye choice is dictated by the most popular blue-excited actuator ChR2. Many relevant sensors capable of excitation by LEDs have peak response when excited at wavelengths longer than that used for ChR2. These optical probes include the green-excited $[Ca^{2+}]_i$ sensors Rhod-4 and the genetically-encoded RGECO [9] and near-infrared V_m sensors, Di-4-ANBDQBS [18] and BeRST1 [19]. The system was designed to work with these probes. The LEDs for exciting the sensors (sLED1, sLED2) and the actuator (aLED) along with bandpass filters used to narrow their spectra to prevent overlap (F_{ex1}, F_{ex2}, F_{actu}) were selected based on the known absorption spectra. Likewise, this determined the selection of the dichroic mirrors (DM1, DM2, DM3) used to combine excitation sources and separate emitted photons before passing through the emission filters in front of the detector. Given the relatively low light levels required and the large selection of economicallypriced light sources, a palette of probes can be used depending on spectral compatibility.

Compatibility of V and $[Ca^{2+}]_i$ probes for dual imaging: cross-talk quantification

Simultaneous imaging using V_m and $[Ca^{2+}]_i$ probes, including the genetically-encoded $[Ca^{2+}]_i$ sensor R-GECO, reliably produces signals (Fig. 2a, c) with minimal crosstalk (Fig. 2b, d), demonstrating the applicability of the platform for multiparameter assessment of function. Crosstalk or “bleed-through” Di-4-ANBDQBS signal can be registered into the $[Ca^{2+}]_i$ channel at this scale, likely due to minor motion artifacts (Fig. 2a, c). However the contribution (SNR and ΔF/F(%)) of this artifactual signal is small compared to the Rhod-4 records. Although Di-4-ANBDQBS was reported to have an excitation spectrum spanning into that of the green LED (sLED2) (Fig. 1a), significant emission was not observed in this preparation. It should be noted that the provided spectra were obtained in ethanol, not in physiological solution [12]. Crosstalk of the remaining probes is negligible, with detector counts close to that of the dark counts of the EMCCD camera. Dual-strobing of dual-stained samples produced signals comparable in morphology to that of single-probe stained samples, both in terms of detector counts and ΔF/F(%). Dual-strobing versus single strobing does produce some crosstalk, where the strong Rhod-4 is seen to bleed into on the V_m channel (without green illumination) in single-stained samples (Fig. 2c, d), most likely the result of the non-zero decay time of the green LED and current source, which can be resolved by reducing the exposure time of the illumination LED. An interesting observation of increase in ΔF/F(%) and SNR for combined BeRST1 and Rhod-4 imaging (Fig. 2c, d)

does not appear to be due to LED bleed-through, as the signal increase is observed under both single and dual strobing conditions and is specific to BeRST1 (not present for Di-4-ANBDQBS), and warrants further investigation. We argue that SNR provides a more informative metric for the quality of the optical signals compared to ΔF/F(%), as seen when comparing V and $[Ca^{2+}]_i$ probes, where the voltage probes may produce lower ΔF/F(%) but the obtained signals have very high SNRs and require minimal post-processing.

Quantification of photobleaching and suitability of V and $[Ca^{2+}]_i$ probes for long-term imaging

To determine the suitability of the synthetic V_m and $[Ca^{2+}]_i$ probes for long term measurements, 5 minute continuous recordings under strobed illumination were obtained in hiPSC-CM samples, optically paced at 0.5Hz (Fig. 3). Bleaching occurs more strongly with Rhod-4 compared to the voltage probes (Fig. 3a, b), with a greater drop in ΔF/F(%) and SNR observed with Rhod-4 when comparing the first 20 seconds and last 20 seconds of the recording (Fig. 3b). BeRST1 exhibited excellent stability over time (hours), without any photo-bleaching within this 5-minute record. Di-4-ANBDQBS had more baseline drift, most likely due to debris entering and exiting the field of view at this microscale; this was present to a lesser extent in BeRST1 samples, as this dye appeared to be less taken up by cellular debris. Even in the presence of bleaching, no major changes in signal morphology were observed with any of the three probes, and in all three cases SNR was high (Fig. 3c). None of the probes used in this study were found to result in any phototoxicity-induced changes in AP/CT morphology within the typical 1–3 hour recording window.

Spatiotemporal imaging

To demonstrate the utility of simultaneous dual imaging using OptoDyCE, hiPSC-CMs were treated with azimilide. The main target effect of this drug is anti-arrhythmic action (slowing rhythm in patients with implantable devices). However, as azimilide blocks K+ ion channels, it can lead to undesired delays in repolarization, excessive prolongation of the action potential and its correlate - QT-interval in the electrocardiogram, and ultimately to repolarization-related arrhythmias; azimilide is considered a high-risk cardiotoxic compound [33] for healthy patients or at elevated doses. Spontaneous and 0.5 Hz optical pacing recordings of hiPSC-CMs labeled with BeRST1 and Rhod-4 were obtained (Fig. 4). Although the azimilide-treated samples, Fig. 4b, showed AP and CT prolongation (known pro-arrhythmic markers) compared to DMSO control, Fig. 4a, no decoupling of voltage and calcium was observed in the global signal, averaged over the whole field of view. However, signals from sufficiently small ROIs at the single-cell scale show such decoupling of V_m and $[Ca^{2+}]_i$ (another pro-arrhythmic feature) in azimilide-treated samples, where abnormal activity in the spontaneous $[Ca^{2+}]_i$ signal is not reflected in the V_m signal. This highlights the need for simultaneous multiparameter measurements and for spatially-resolved imaging, which is particularly useful to distinguish between and gain mechanistic insights into calcium-triggered arrhythmic events vs. classic electrical instabilities [34]. Pacing can be effective in reducing this voltage-calcium decoupling and in suppressing abnormal calcium release events, yet the drug-induced AP prolongation limits the rates at which the system remains stable and responsive. Fig. 4c shows summary of results with azimilide treatment compared to control, namely significantly reduced frequency of spontaneous activations

($p<0.01$) and significantly prolonged action potential duration (APD) at 90% and at 50% recovery, $p<0.01$, for optically-paced records. Optical stimulation is essential for scalable measurements of drug-induced chages in the morphology of the action potentials and the calcium transients; even when a drug may act on the optogenetic actuator (ChR2), this has minimal effect on the measured APD, CTD, as we have suggested previously [5]. Optogenetic pacing is limited however, when probing changes in excitability if the tested drug has significant effects on ChR2.

Effects of excitation irradiance on SNR

Although ΔF/F% is the most commonly reported quantification of signal quality in optical mapping, SNR plays a larger role in signal processing and feature detection. In this study with the presented platform, all probes showed excellent SNR. Even for very low light levels and low concentrations of staining, the optical signals were usable without filtering. The three probes characterized here were capable of SNR of 100 or more. Varying incident irradiance of the green LED for Rhod-4 excitation (Fig. 5a) shows that SNR only scales directly with irradiance until 0.3 mW/mm^2, where oversaturation of pixels results in decreasing SNR. Multiple variables can affect the irradiances at which such saturation will be reached, including factors unrelated to the dyes used, e.g. camera pixel well depth and EMCCD gain. It should be noted that the LED was set to only 30% maximum power (0.53 mW/mm^2) before the whole detector area was oversaturated for these samples. Although ChR2 kinetics has been reported to be affected by green (520 nm) wavelengths [35], mostly leading to accelerated closing of ChR2, peak SNR of Rhod-4 appears to occur at relatively low irradiances and thus excitation of the probe should not engage ChR2. Both Di-4-ANBDQBS and BeRST1 show similar profiles for irradiance (Fig. 5b, c). SNR for BeRST1 plateaus around 2.8 mW/mm^2, while Di-4-ANBDQBS decreases in SNR at high LED irradiances > 5.45 mW/mm^2 due to pixel oversaturation in areas with dye-containing cellular debris. For both V_m probes, oversaturation of the whole detector area did not occur before the LED power was at maximum (6.6 mW/mm^2). For most recordings, the relevant excitation irradiances for the calcium probes were lower than those for voltage probes, ranging from 0.46 – 0.53 mW/mm^2 for Rhod-4 and 1.4 – 2.5 mW/mm^2 for Di-4-ANBDQBS and BeRST1, as seen in (Fig. 5) and (Fig. 2c).

DISCUSSION

Here we demonstrate that OptoDyCE can be adapted to perform simultaneous dual imaging of V_m and $[Ca^{2+}]_i$ combined with optogenetic actuation using ChR2 to interrogate complex spatiotemporal phenomena in hiPSC-CMs. Although dual imaging approaches using a single detector and two LED sources have been proposed and employed previously, these systems relied on an “off-axis” configuration, where the illumination and detection paths do not overlap [31, 36]. While dual “on-axis” approaches have been performed, they typically rely on two-detector configurations [37–39]. Considering that the photodetector (camera) is the most expensive component in these all-optical systems, the “on axis” temporal multiplexing approach presented here offers a particularly attractive solution. Additionally, none of the previously published techniques have demonstrated combined simultaneous measurements of V_m and $[Ca^{2+}]_i$ with optogenetic stimulation. Dual imaging using combined genetically-

encoded sensors and actuators has been used to perform drug screening in hiPSC-CMs [6], however it required two cameras and two light sources for readout, and the actuators and sensors were not coexpressed in the same cells. Approaches using genetically-encoded probes and actuators are of interest in long-term monitoring of chronic drug treatment over hours and days, such as kinase-effecting drugs, where synthetic probes may not be ideal. OptoDyCE employs simple off-the-shelf optical components and uses temporal multiplexing of optical sensing by high-speed gating of LED illumination [30] not possible with traditional sources. Imaging of complex phenomena can be performed using a single detector thus achieving a cost-effective yet powerful configuration capable of acquiring high-content information. The “on-axis” aspect of the system makes it amenable to miniaturization and integration with micro-endoscopic systems for all-optical *in vivo* applications [40].

As novel imaging technologies continue to be developed for use in cardiac electrophysiology, quality metrics for both the imaging system and the optical reporters must be established. Although optical mapping commonly uses ΔF/F% to determine the quality of a fluorescent reporter, we suggest that SNR provides a better metric of signal detectability and signal quality, which is more commonly used in the context of high-speed imaging. Given the need for recording speeds >200 fps (and thus short exposure times), signals with small (<10%) dynamic changes can be more susceptible to noise (e.g. detector and photon noise), requiring temporal and spatial filtering, which affects signal fidelity. When variability in the signal baseline is not taken into account, as with DF/F%, signal quality can be incorrectly represented, as seen when comparing V_m and $[Ca^{2+}]_i$ probes (Fig. 2c, d). Additionally, we observe that ΔF/F% varies more than SNR across samples, most likely due to variability in dye loading and illumination intensity. Probes producing higher SNRs lessen the need for filtering signals, which both maintains signal fidelity and reduces computational requirements. It also reduces the strict dependence on expensive, high-sensitivity cameras and large numerical aperture (NA) optics. The recently synthesized near-infrared dye BeRST1 shows very high quality signals by both metrics and yields an impressive SNR, comparable to those for traditional $[Ca^{2+}]_i$ probes. Di-4-ANBDQBS also provides a good readout. It is important to note that in their current formulations, BeRST1 required an order of magnitude lower concentration compared to Di-4-ANBDQBS (1 mM compared to 35 mM) to produce the signals presented here. However, further improvement of the SNR for Di-4-ANBDQBS and removal of the baseline drift may be possible by leveraging its capability as an excitation-ratiometric probe [18]. When coupled with suitable photodetectors, sensitive in the NIR, these newer voltage sensors represent an important contribution to optical electrophysiology. They will fit a commercial need, as exemplified by recent developments and/or usage of NIR probes by several companies.

In all-optical electrophysiology, spectral compatibility and complex interactions between optical actuators and sensors present challenges when multiple variables need to be monitored simultaneously. Here, we demonstrate that simple solutions can be pursued, with minimal crosstalk, Fig. 2. Nevertheless, full characterization of potential interferences likely need to be conducted for each considered set of optical actuators and sensors, especially for genetically-encoded sensors, as ChR2 excitation is known to have the potential to photo-switch these sensors to different fluorescent states – a phenomenon that is enhanced at

higher irradiance levels. For example, newer red-shifted GECI, jRCaMP1 and jRGECO1, were developed to minimize such effects [41].

The OptoDyCE platform is compatible with both synthetic and genetically-encoded sensors and allows for short-term and long-term all-optical control of samples with optogenetic actuators. In particular, the contactless nature makes the platform suitable for high-throughput measurements of hiPSC-CMs, allowing dissection of the V_m - $[Ca^{2+}]_i$ dynamics. Although in this study we have only demonstrated OptoDyCE as a tool for measuring optically reported V_m and $[Ca^{2+}]_i$ in hiPSC-CMs, the platform is suitable for recording any optically-measurable parameter (e.g. organelle-based ion concentrations, pH, contraction, etc.) and is impartial to the studied cell-type, allowing for the interrogation of compatible samples of different geometries, including 2D monolayers and small-thickness 3D tissue constructs for which light penetration is not limiting [5]. As new actuators and sensors (both synthetic and genetically-encoded) become available, they can be easily screened with and then integrated into the platform. The ability to provide dynamic pacing and high-throughput recording on an all-optical “on-axis” platform, easily adaptable to changing technologies, makes this an economical tool for better understanding of cardiac electrophysiology *in vitro* and *in vivo*. In the current *in vitro* context, it not only has the potential to improve cardiotoxicity testing, but also offers a cost-effective means of automation and phenotypic testing of hiPSC-CMs to accelerate the wider adoption of stem cell technologies in drug discovery and development, disease modeling, and personalized medicine.

ACKNOWLEDGEMENTS

This work was supported in part by the National Institutes of Health (grant numbers R01HL111649, R21 EB026152 to E.E.; R35GM119855 to E.W.M.) and the National Science Foundation (grants 1623068, 1705645, 1830941, 1827535 to E.E.). E.W.M. acknowledges support from the Alfred P. Sloan Foundation (FG-2016–6359) and the March of Dimes (5-FY16–65). S.B. was supported in part by NIH T32GM066698. G.O. was supported in part by a Gilliam Fellowship for Advanced Study by the Howard Hughes Medical Institute.

REFERENCES

1. Entcheva E, and Bub G (2016). All-optical control of cardiac excitation: combined highresolution optogenetic actuation and optical mapping. J Physiol 594, 2503–2510. [PubMed: 26857427]
2. Entcheva E, and Bien H (2006). Macroscopic optical mapping of excitation in cardiac cell networks with ultra-high spatiotemporal resolution. Prog.Biophys.Mol.Biol 92, 232–257. [PubMed: 16330086]
3. Herron TJ, Lee P, and Jalife J (2012). Optical imaging of voltage and calcium in cardiac cells & tissues. Circ Res 110, 609–623. [PubMed: 22343556]
4. Nagel G, Szellas T, Huhn W, Kateriya S, Adeishvili N, Berthold P, Ollig D, Hegemann P, and Bamberg E (2003). Channelrhodopsin-2, a directly light-gated cation-selective membrane channel. Proc Natl Acad Sci U S A 100, 13940–13945. [PubMed: 14615590]
5. Klimas A, Ambrosi CM, Yu J, Williams JC, Bien H, and Entcheva E (2016). OptoDyCE as an automated system for high-throughput all-optical dynamic cardiac electrophysiology. Nature communications 7, 11542.
6. Dempsey GT, Chaudhary KW, Atwater N, Nguyen C, Brown BS, McNeish JD, Cohen AE, and Kralj JM (2016). Cardiotoxicity screening with simultaneous optogenetic pacing, voltage imaging and calcium imaging. J Pharmacol Toxicol Methods 81, 240–250. [PubMed: 27184445]
7. McKeithan WL, Savchenko A, Yu MS, Cerignoli F, Bruyneel AAN, Price JH, Colas AR, Miller EW, Cashman JR, and Mercola M (2017). An Automated platform for assessment of congenital and

drug-induced arrhythmia with hipsc-derived cardiomyocytes. Frontiers in physiology 8, 1–12. [PubMed: 28154536]

8. Burton RAB, Klimas A, Ambrosi CM, Tomek J, Corbett A, Entcheva E, and Bub G (2015). Optical control of excitation waves in cardiac tissue. Nature photonics 9, 813–816. [PubMed: 27057206]
9. Zhao Y, Araki S, Wu J, Teramoto T, Chang YF, Nakano M, Abdelfattah AS, Fujiwara M, Ishihara T, Nagai T, et al. (2011). An Expanded Palette of Genetically Encoded Ca2+ Indicators. Science 333, 1888–1891. [PubMed: 21903779]
10. Chen T-W, Wardill TJ, Sun Y, Pulver SR, Renninger SL, Baohan A, Schreiter ER, Kerr RA, Orger MB, Jayaraman V, et al. (2013). Ultrasensitive fluorescent proteins for imaging neuronal activity. Nature 499, 295–300. [PubMed: 23868258]
11. Mutoh H, and Knopfel T (2013). Probing neuronal activities with genetically encoded optical indicators: from a historical to a forward-looking perspective. Pflugers Arch 465, 361–371. [PubMed: 23271451]
12. Hochbaum DR, Zhao Y, Farhi SL, Klapoetke N, Werley CA, Kapoor V, Zou P, Kralj JM, Maclaurin D, Smedemark-Margulies N, et al. (2014). All-optical electrophysiology in mammalian neurons using engineered microbial rhodopsins. Nature methods 11, 825–833. [PubMed: 24952910]
13. Abdelfattah AS, Farhi SL, Zhao Y, Brinks D, Zou P, Ruangkittisakul A, Platisa J, Pieribone VA, Ballanyi K, Cohen AE, et al. (2016). A Bright and Fast Red Fluorescent Protein Voltage Indicator That Reports Neuronal Activity in Organotypic Brain Slices. J Neurosci 36, 2458–2472. [PubMed: 26911693]
14. Xu F, Shi DQ, Lau PM, Lin MZ, and Bi GQ (2018). Excitation wavelength optimization improves photostability of ASAP-family GEVIs. Mol Brain 11, 32. [PubMed: 29866136]
15. Chamberland S, Yang HH, Pan MM, Evans SW, Guan S, Chavarha M, Yang Y, Salesse C, Wu H, Wu JC, et al. (2017). Fast two-photon imaging of subcellular voltage dynamics in neuronal tissue with genetically encoded indicators. eLife 6.
16. St-Pierre F, Marshall JD, Yang Y, Gong Y, Schnitzer MJ, and Lin MZ (2014). High-fidelity optical reporting of neuronal electrical activity with an ultrafast fluorescent voltage sensor. Nat Neurosci.
17. Lee EEL, and Bezanilla F (2017). Biophysical Characterization of Genetically Encoded Voltage Sensor ASAP1: Dynamic Range Improvement. Biophys J 113, 2178–2181. [PubMed: 29108650]
18. Matiukas A, Mitrea BG, Qin M, Pertsov AM, Shvedko AG, Warren MD, Zaitsev AV, Wuskell JP, Wei MD, Watras J, et al. (2007). Near-infrared voltage-sensitive fluorescent dyes optimized for optical mapping in blood-perfused myocardium. Heart Rhythm 4, 1441–1451. [PubMed: 17954405]
19. Huang Y-L, Walker AS, and Miller EW (2015). A Photostable Silicon Rhodamine Platform for Optical Voltage Sensing. Journal of the American Chemical Society 137, 10767–10776. [PubMed: 26237573]
20. Fertig N, and Farre C (2010). Renaissance of ion channel research and drug discovery by patch clamp automation. Future medicinal chemistry 2, 691–695. [PubMed: 21426196]
21. Li X, Zhang R, Zhao B, Lossin C, and Cao Z (2016). Cardiotoxicity screening: a review of rapid-throughput in vitro approaches. Arch Toxicol 90, 1803–1816. [PubMed: 26676948]
22. Quach B, Krogh-Madsen T, Entcheva E, and Christini DJ (2018). Light-Activated Dynamic Clamp Using iPSC-Derived Cardiomyocytes. Biophys J 115, 2206–2217. [PubMed: 30447994]
23. Yamamoto W, Asakura K, Ando H, Taniguchi T, Ojima A, Uda T, Osada T, Hayashi S, Kasai C, Miyamoto N, et al. (2016). Electrophysiological Characteristics of Human iPSC-DerivedCardiomyocytes for the Assessment of Drug-Induced Proarrhythmic Potential. PLoS One 11, e0167348. [PubMed: 27923051]
24. Blinova K, Stohlman J, Vicente J, Chan D, Johannesen L, Hortigon-Vinagre MP, Zamora V, Smith G, Crumb WJ, Pang L, et al. (2017). Comprehensive Translational Assessment ofHuman-Induced Pluripotent Stem Cell Derived Cardiomyocytes for Evaluating Drug-InducedArrhythmias. Toxicological sciences : an official journal of the Society of Toxicology 155, 234–247. [PubMed: 27701120]
25. Harris K, Aylott M, Cui Y, Louttit JB, McMahon NC, and Sridhar A (2013). Comparison of electrophysiological data from human-induced pluripotent stem cell-derived cardiomyocytes to

functional preclinical safety assays. Toxicological sciences : an official journal of the Society of Toxicology 134, 412–426. [PubMed: 23690542]

26. Ambrosi CM, Boyle PM, Chen K, Trayanova NA, and Entcheva E (2015). Optogenetics-enabled assessment of viral gene and cell therapy for restoration of cardiac excitability. Scientific reports 5, 17350. [PubMed: 26621212]
27. Ambrosi CM, and Entcheva E (2014). Optogenetic Control of Cardiomyocytes via ViralDelivery. Methods Mol Biol 1181, 215–228. [PubMed: 25070340]
28. Chung CY, Bien H, Sobie EA, Dasari V, McKinnon D, Rosati B, and Entcheva E (2011). Hypertrophic phenotype in cardiac cell assemblies solely by structural cues and ensuing self-organization. Faseb J 25, 851–862. [PubMed: 21084696]
29. Jia Z, Valiunas V, Lu Z, Bien H, Liu H, Wang HZ, Rosati B, Brink PR, Cohen IS, andEntcheva E (2011). Stimulating Cardiac Muscle by LightClinical Perspective CardiacOptogenetics by Cell Delivery. Circulation: Arrhythmia and Electrophysiology 4, 753–760. [PubMed: 21828312]
30. Entcheva E, Kostov Y, Tchernev E, and Tung L (2004). Fluorescence imaging of electricalactivity in cardiac cells using an all-solid-state system. IEEE Trans.Biomed.Eng 51, 333–341. [PubMed: 14765706]
31. Lee P, Bollensdorff C, Quinn TA, Wuskell JP, Loew LM, and Kohl P (2011). Single-sensor system for spatially resolved, continuous, and multi-parametric optical mapping of cardiac tissue. Heart Rhythm 8, 1482–1491. [PubMed: 21459161]
32. Bien H, Yin L, and Entcheva E (2006). Calcium instabilities in Mammalian cardiomyocyte networks. Biophys.J. 90, 2628–2640. [PubMed: 16399841]
33. Gintant G, Sager PT, and Stockbridge N (2016). Evolution of strategies to improve preclinical cardiac safety testing. Nat Rev Drug Discov 15, 457–471. [PubMed: 26893184]
34. Shiferaw Y, Sato D, and Karma A (2005). Coupled dynamics of voltage and calcium in paced cardiac cells. Phys Rev E Stat Nonlin Soft Matter Phys 71, 021903. [PubMed: 15783348]
35. Bamann C, Kirsch T, Nagel G, and Bamberg E (2008). Spectral characteristics of the photocycle of channelrhodopsin-2 and its implication for channel function. J Mol Biol 375, 686–694. [PubMed: 18037436]
36. Lee P, Klos M, Bollensdorff C, Hou L, Ewart P, Kamp TJ, Zhang J, Bizy A, Guerrero-Serna G, Kohl P, et al. (2012). Simultaneous Voltage and Calcium Mapping of Genetically Purified Human Induced Pluripotent Stem Cell-Derived Cardiac Myocyte Monolayers. Circ Res.
37. Fast VG, and Ideker RE (2000). Simultaneous optical mapping of transmembrane potentialand intracellular calcium in myocyte cultures. J Cardiovasc Electrophysiol 11, 547–556. [PubMed: 10826934]
38. Laurita KR, and Singal A (2001). Mapping action potentials and calcium transients simultaneously from the intact heart. Am J Physiol Heart Circ Physiol 280, 2053–2060.
39. Choi BR, and Salama G (2000). Simultaneous maps of optical action potentials and calciumtransients in guinea-pig hearts: mechanisms underlying concordant alternans. J Physiol 529 Pt 1, 171–188. [PubMed: 11080260]
40. Klimas A, and Entcheva E (2014). Toward microendoscopy-inspired cardiac optogenetics invivo: technical overview and perspective. J Biomed Opt 19, 80701.
41. Dana H, Mohar B, Sun Y, Narayan S, Gordus A, Hasseman JP, Tsegaye G, Holt GT, Hu A, Walpita D, et al. (2016). Sensitive red protein calcium indicators for imaging neural activity. eLife 5.

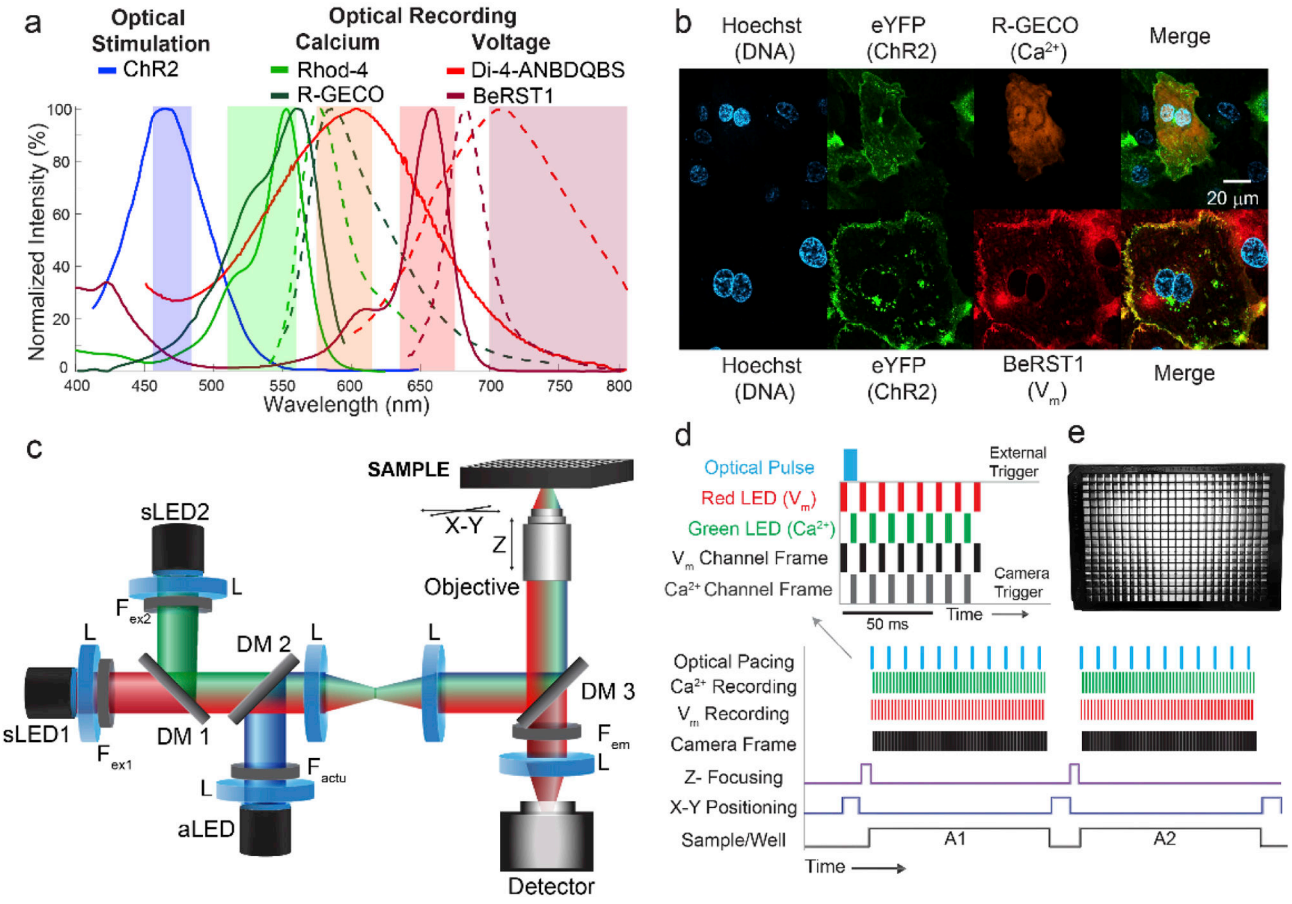

Figure 1.

"On axis" multimodal all-optical cardiac electrophysiology based on the OptoDyCE platform. (a) Spectrally-compatible synthetic and genetically-encoded fluorescent reporters of V_m and $[Ca^{2+}]_i$ can be combined with optogenetic actuators to perform all-optical interrogation of hiPSC-CMs. (b) Fluorescent images of hiPSC-CMs treated with the nuclear stain Hoechst (blue) show successful expression of both eYFP-tagged ChR2 (green) with R-GECO (orange), a genetically encoded $[Ca^{2+}]_i$ sensor, while the V_m dye BeRST1 (red) shows strong membrane localization. Scale bar is 20 mm. (c) OptoDyCE can readily perform simultaneous imaging of V_m and $[Ca^{2+}]_i$ using a single detector through 'strobing' the sensing LEDs (sLED1 and sLED2), which are temporally multiplexed or gated by the camera (d). Due to the contactless nature of all-optical interrogation, this approach allows for automated recording of standard multi-well plates (e).

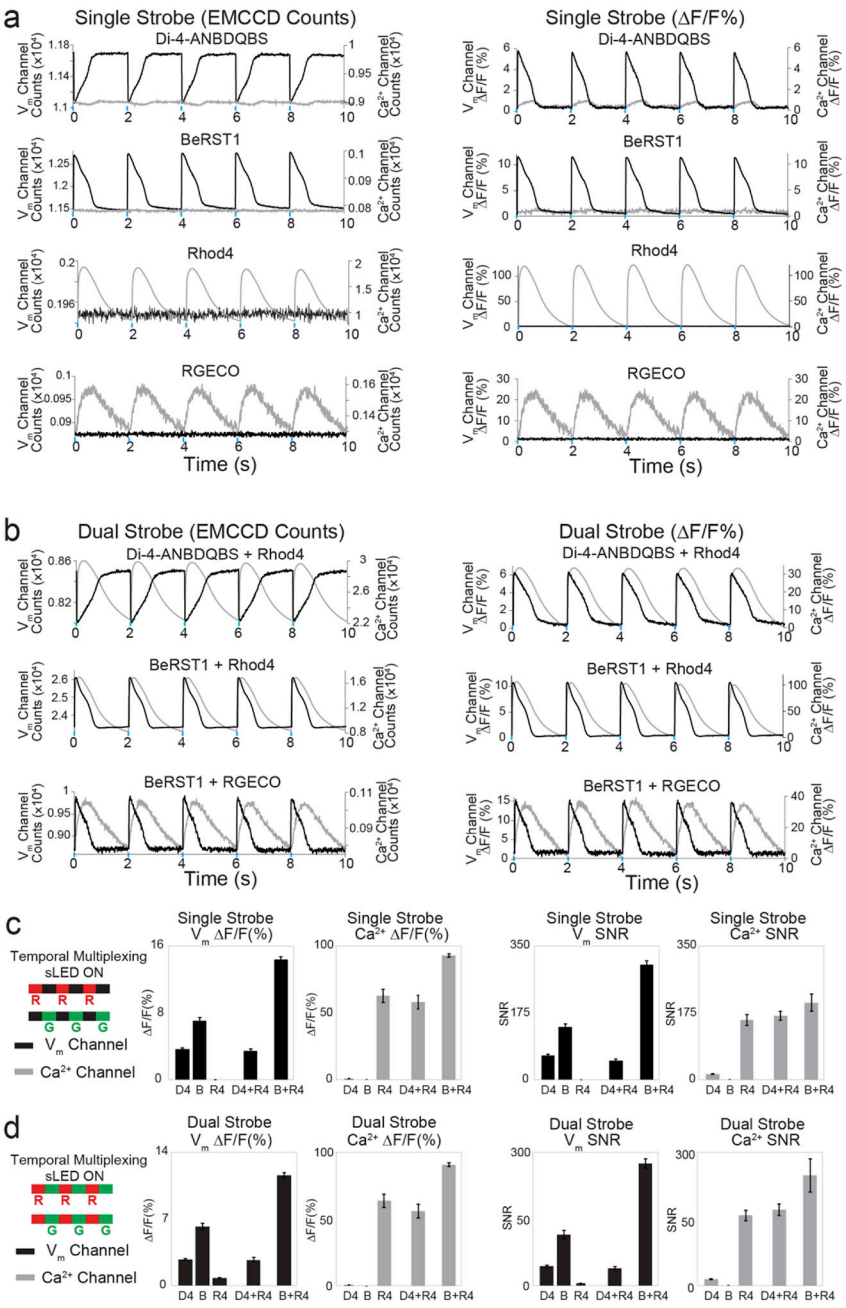

Figure 2.

Investigation of compatibility of V_m and $[Ca^{2+}]_i$ probes and cross-talk. OptoDyCE can simultaneously measure V and $[Ca^{2+}]_i$ using Di-4-ANBDQBS (D4) or BeRST1 (B) combined with Rhod-4 (R4) or RGECO (RG) under strobed illumination of hiPSC-CMs, optically paced at 0.5Hz. V and $[Ca^{2+}]_i$ channel denote recordings from frames gated to the excitation source (sLED) of the respective probes. Red (R) denotes recordings from frames synchronized to sLED1 (V_m) and green (G) for sLED2 ($[Ca^{2+}]_i$). Signals are given in terms of EMCCD detector counts (left) and ΔF/F(%) (right) for both single (a) and dual (b) strobe conditions. Single strobe illumination of single-probe samples (a, left) show counts close to

the detector dark counts for B, R4, and RG while red-excited D4 is seen to produce a motion-artifact signal on the $[Ca^{2+}]_i$ channel (green illumination). Comparison of ΔF/F(%) to SNR for both single-strobe and dual-strobe illumination (N = 5, 6 distinct samples per case) (c,d) show that even if present, the SNR of the minor crosstalk is much smaller than that of the desired signal for the respective channel. Irradiances were kept the same for a particular wavelength (dye type) within a plate, but were adjusted between plates to account for differences in cell plating and dye loading and to optimize SNR; red LED: 1.4 to 2.5 mW/mm^2, green LED 0.46 to 0.53 mW/mm^2.

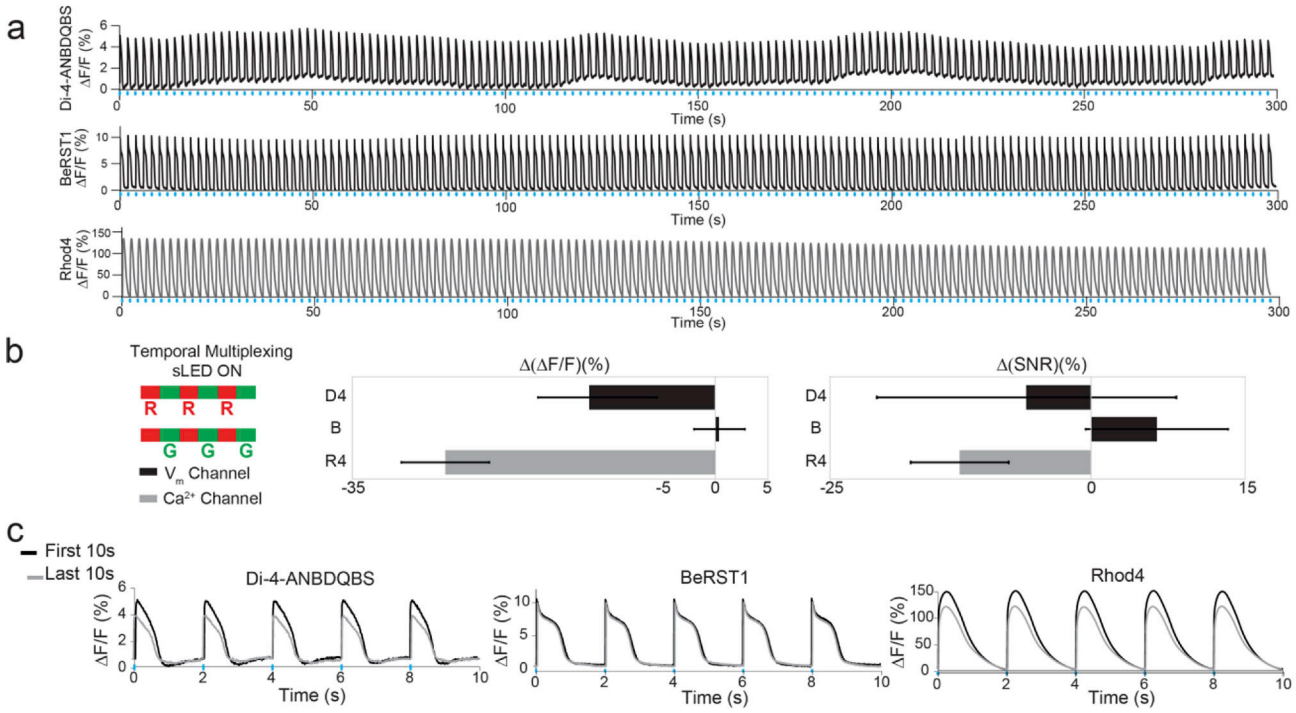

Figure 3.

Stability and photobleaching of V_m and $[Ca^{2+}]_i$ probes. Strobed illumination for 5 minutes combined with optical pacing exhibits minor photobleaching for di-4-ANBDQBS (D4) and Rhod4 (R4), but no photobleaching for BeRST1 (B) (a) with stronger bleaching observed in Rhod4 (R4) when comparing the percent change between the first and last 20 seconds of the recording for both ΔF/F(%) (given as Δ (ΔF/F)) and SNR (given as Δ (SNR)) (N=4 samples) (b). Additionally, no major changes in AP/CT morphology are observed after 5 minutes of recording (c).

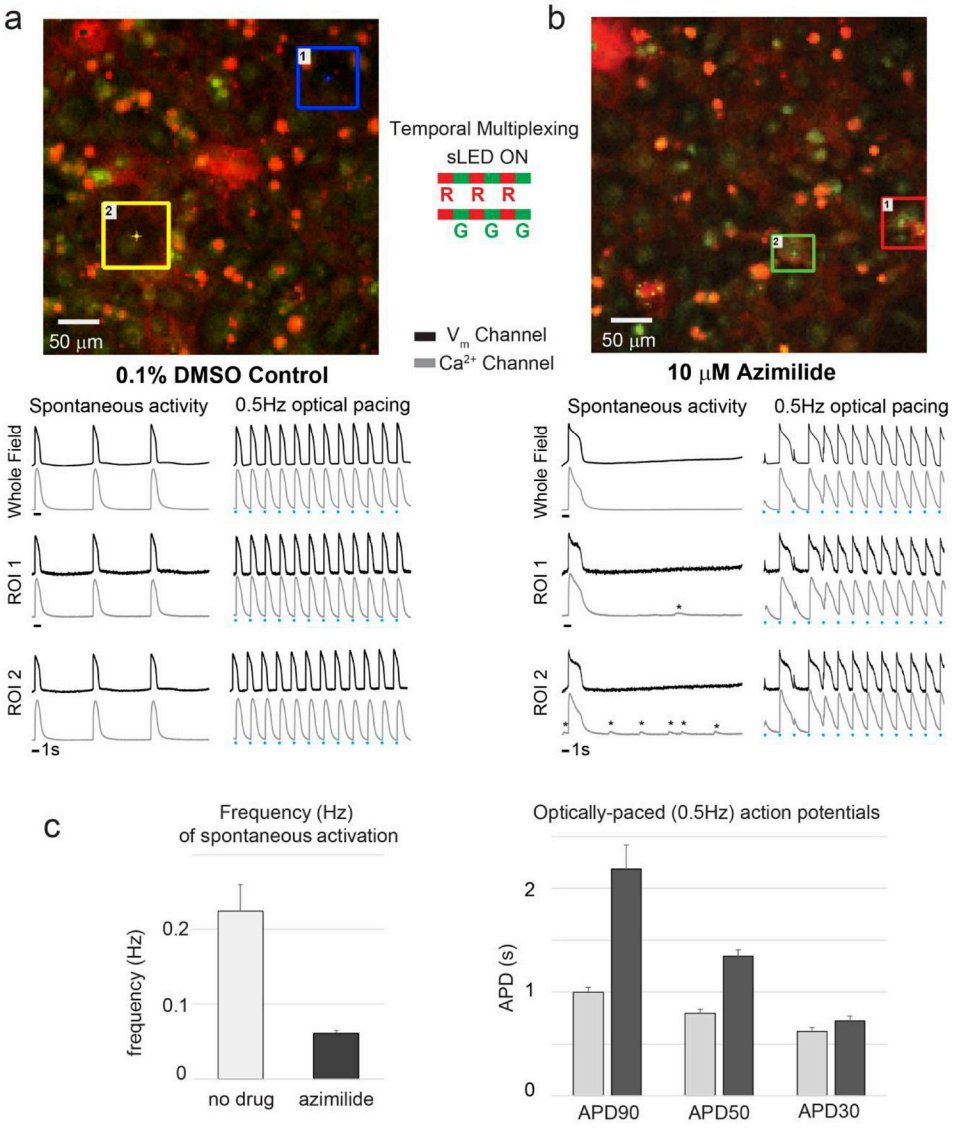

Figure 4.

Dual imaging of V_m and $[Ca^{2+}]_i$ probes to capture sub-cellular events for pro-arrhythmia prediction. hiPSC-CM samples stained with BeRST1 and Rhod-4 were treated with 0.1% DMSO (a) or 10 μM azimilide (b), a known proarrhythmic compound. Averaging over the whole field, azimilide is seen to prolong both the spontaneous and paced action potential and calcium transient, a known marker of proarrhythmic risk. Signals from single-cell ROIs show decoupling of V_m and $[Ca^{2+}]_i$ in azimilide treated samples (*asterisks), another indicator of pro-arrhythmic risk, not detectable in the global signal. (c) Comparison of parameters for no-drug samples (N = 5) and azimilide (N = 6) - frequency of spontaneous activations (Hz) is decreased by azimilide; optically-paced (0.5Hz) responses show prolonged action potential duration (APD) at 90, 50 and 30%.

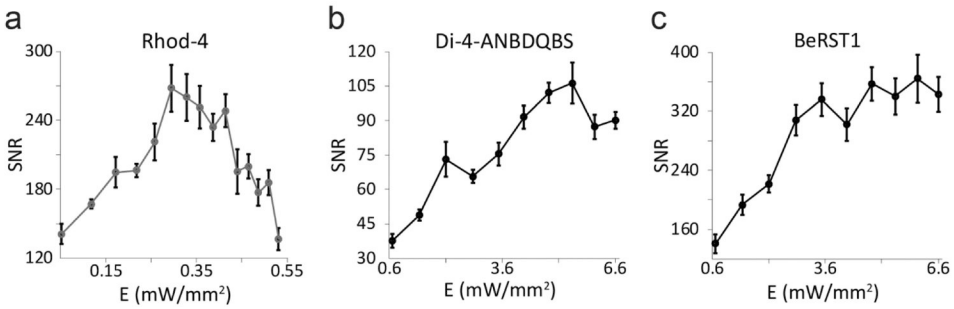

Figure 5.

Effects of excitation irradiance on SNR of V_m and $[Ca^{2+}]_i$ probes. SNR for Rhod-4 (a), Di-4-ANBDQBS (b), and BeRST1 (c) were calculated for a single hiPSC-CM sample optically paced at 0.5 Hz.